Unusual One-Dimensional Ladder Structures Containing Divalent Europium and the Tetracyanometalates $Ni(CN)_4^{2-}$ and $Pt(CN)_4^{2-}$

David W. Knoeppel and Sheldon G. Shore*

Department of Chemistry, The Ohio State University, Columbus, Ohio 43210

Received March 28, 1996[⊗]

The heterobimetallic one-dimensional arrays $\{(DMF)_4EuNi(CN)_4\}_\infty$ and $\{(DMF)_4EuPt(CN)_4\}_\infty$ were prepared from the metathesis of $(NH_3)_xEuCl_2$ with $K_2Ni(CN)_4$ and $K_2Pt(CN)_4$, respectively, in DMF. The analogous reaction between $(NH_3)_xYbCl_2$ and $K_2Ni(CN)_4$ in DMF or DMA resulted in oxidation of Yb^{2+} and reduction of $Ni(CN)_4^{2-}$ to give the previously reported dinuclear Ni(I) anion $Ni_2(CN)_6^{4-}$. Single-crystal X-ray diffraction analysis revealed that $\{(DMF)_4EuNi(CN)_4\}_\infty$ and $\{(DMF)_4EuPt(CN)_4\}_\infty$ form isostructural one-dimensional "ladder" arrays through isocyanide linkages (Eu−NC−M). Crystal data for $\{(DMF)_4EuNi(CN)_4\}_\infty$: triclinic space group $P\bar{1}$, $a = 8.902(2)$ Å, $b = 10.947(2)$ Å, $c = 12.464(4)$Å, $\alpha = 82.99(2)°$, $\beta = 86.86(2)°$, $\gamma = 84.92(2)°$, $Z = 2$. Crystal data for $\{(DMF)_4EuPt(CN)_4\}_\infty$: triclinic space group $P\bar{1}$, $a = 8.918(1)$ Å, $b = 11.160(2)$ Å, $c = 12.480(2)$ Å, $\alpha = 83.27(2)°$, $\beta = 86.84(1)°$, $\gamma = 83.71(2)°$, $Z = 2$. Electrical conductance measurements and infrared spectra of DMF solutions of these one-dimensional arrays revealed that solvent-separated ion pairs are predominant in solution.

Introduction

All of the rare earth metals form ions with a 2+ oxidation state,[1] but only three of those elements, Sm, Eu, and Yb, form stable 2+ cations under normal chemical conditions. In comparison to that of their more thermodynamically stable trivalent counterparts, the chemistry of these ions has not been explored a great deal. Our focus has been to investigate the coordination chemistry of the divalent lanthanides with a variety of Lewis bases, including transition metal anions,[2] for possible uses as heterobimetallic catalysts or as precursors to oxide-supported heterobimetallic particles.

Our initial studies employed nucleophilic transition metal carbonylate anions. These anions are characterized as soft Lewis bases and excellent nucleophiles.[3] Coupled with the fact that the divalent lanthanides are softer Lewis acids than their trivalent counterparts,[4] ion-paired complexes are expected. Ion-paired complexes can result from rarely observed lanthanide−transition metal bonds[2b,c,e,5] or from the more commonly observed isocarbonyl linkages.[6] In cases where the transition metal anions are not sufficiently nucleophilic, the lanthanide ions are surrounded by coordinating solvents such as acetonitrile, pyridine, and diglyme to yield solvent-separated ion pairs.[2a,d,e,7] Unfortunately, many of the transition metal carbonylate anions are extremely air sensitive and isolation of such complexes can be very difficult. With this in mind, we set out to investigate the use of alternative transition metal anions that might prove to be more robust and provide us with desired ion-paired complexes. We chose transition metal cyanides with the prospects that the bidentate cyanide ion would bridge both the transition metal and the lanthanide ion. Of the many tetracyanometalate(II) (metal = Ni, Pd, Pt) complexes known, only two teracyanopalladate(II) structures have been reported that employ lanthanide cations.[8,9] However, no synthetic information nor structural details were given. A series of rare earth complexes having the general formula $Ln_2[Pt(CN)_4]_3 \cdot XH_2O$ ($X = 18$, 21) have also been reported.[10] Spectroscopic evidence and preliminary X-ray data suggest that these complexes adopt a quasi-one-dimensional structure common to the tetracyanoplatinates(II).

We report here the reactions of $LnCl_2$ and $K_2M(CN)_4$ (Ln = Yb, Eu; M = Ni, Pt) in *N*,*N*-dimethylformamide (DMF) or *N*,*N*-dimethylacetamide (DMA). Details of the synthesis and characterization of $[(DMF)_4EuNi(CN)_4]_\infty$ and $[(DMF)_4EuPt(CN)_4]_\infty$ are described. To our knowledge, these are the first reported structures containing divalent lanthanides and transition metal cyanoates. The crystal structures of these isostructural complexes revealed that each teracyanometalate anion bridges three europium atoms to form a one-dimensional ladder. We also believe these are the first structural examples of this class of tetracyanometalates where three of the four bidentate cyanide ligands are involved as bridges between two metal atoms.

[⊗] Abstract published in *Advance ACS Abstracts,* August 15, 1996.

(1) McClure, D. S.; Kiss, Z. *J. Chem. Phys.* **1963**, *39*, 3251.
(2) (a) White, J. P., III; Deng, H.; Boyd, E. P.; Gallucci, J.; Shore, S. G. *Inorg. Chem.* **1994**, *33*, 1685. (b) Deng, H.; Shore, S. G. *J. Am. Chem. Soc.* **1991**, *113*, 8538. (c) Deng, H.; Chun, S.; Florian, P.; Grandinetti, P. J.; Shore, S. G. *Inorg. Chem.* **1996**, *35*, 1747. (d) White, J. P., III. Ph.D. dissertation, The Ohio State University, Columbus, OH, 1990. (e) Deng, H. Ph.D. Dissertation, The Ohio State University, Columbus, OH, 1991. (f) Knoeppel, D. W.; Shore, S. G. *Inorg. Chem.* **1996**, *35*, 3891. (g) Knoeppel, D. W. Ph.D. dissertation, The Ohio State University, Columbus, OH, 1995.
(3) Ellis, J. E. *Adv. Organomet. Chem.*, **1990**, *31*, 1.
(4) Pearson, R. G. *J. Am. Chem. Soc.* **1963**, *85*, 3533.
(5) (a) Magomedov, G. K; Voskoboynikov, A. Z.; Chuklanova, E. B.; Gusev, A. I.; Beletskaya, I. P. *Metalloorg. Khim.* **1990**, *3*, 706. (b) Beletskaya, I. P.; Voskoboynikov, A. Z.; Chuklanova, E. B.; Kirillova, N. I.; Shestakova, A. K.; Parshina, I. N.; Gusev, A. I.; Magomedov, G. K.-I. *J. Am. Chem. Soc.* **1993**, *115*, 3156.
(6) (a) Tilley, T. D.; Andersen, R. A. *J. Chem. Soc., Chem. Commun.* **1981**, 985. (b) Tilley, T. D.; Andersen, R. A. *J. Am. Chem. Soc.* **1982**, *104*, 1772. (c) Boncella, J. M.; Andersen, R. A. *Inorg. Chem.* **1984**, *23*, 432. (d) Boncella, J. M.; Andersen, R. A. *J. Chem. Soc., Chem. Commun.* **1984**, 809. (e) Recknagel, A.; Steiner, A.; Brooker, S.; Stalke, D.; Edelmann, F. *Chem. Ber.* **1991**, *124*, 1373.
(7) (a) Evans, W. J.; Bloom, I.; Grate, J. W.; Hughes, L. A.; Hunter, W. E.; Atwood, J. L. *Inorg. Chem.* **1985**, *24*, 4620. (b) Beletskaya, I. P.; Voskoboynikov, A. Z.; Chuklanova, E. B.; Gusev, A. I.; Magomedov, G. K. *Metalloorg. Khim.* **1988**, *1*, 1383.
(8) Klement, U. *Z. Kristallogr.* **1993**, *208*, 285.
(9) Klement, U. *Z. Kristallogr.* **1993**, *208*, 288. Since no structural details were provided in this communication, crystallographic data and atomic coordinates that were available were used to calculate bond distances and angles for comparisons.
(10) Glieman, G.; Yersin, H. *Struct. Bonding* **1985**, *62*, 87 and references therein.

S0020-1669(96)00337-0 CCC: $12.00

Results and Discussion

The Yb^{2+} ion is intermediate in stability between those of Eu^{2+} (the most stable) and Sm^{2+} (the least stable), but its diamagnetic behavior ($4f^{14}$) offers no hindrance to NMR spectral characterization. In addition, it is the least expensive of the three metals. Attempts to synthesize the divalent ytterbium complex $(solv)_xYbNi(CN)_4$ (solv = DMF, DMA) via the metathesis of equimolar quantities of $YbCl_2$ and $K_2Ni(CN)_4$ were unsuccessful (eqs 1 and 2). Within 30 min of mixing the

$$YbCl_2 + K_2Ni(CN)_4 \xrightarrow{DMF} \underset{\mathbf{1}}{\{(DMF)_{10}Yb_2[Ni(CN)_4]_3\}_\infty} + Ni_2(CN)_6^{4-} + KCl \quad (1)$$

$$YbCl_2 + K_2Ni(CN)_4 \xrightarrow{DMA} \underset{\mathbf{2}}{\{(DMA)_4Yb[Ni(CN)_4]Cl\}_\infty} + Ni_2(CN)_6^{4-} + KCl \quad (2)$$

reactants, the orange solution of solvated $YbCl_2$ and $K_2Ni(CN)_4$ begins to turn yellow with the precipitation of KCl as well as a red-brown solid. After several days of stirring, filtration and subsequent crystallization from the yellow filtrate solution result in the isolation of light-yellow solids. Solid state and solution infrared spectra as well as ^{13}C NMR spectra of these yellow crystals are identical to those of the trivalent ytterbium solid state one-dimensional arrays $\{(DMF)_{10}Yb_2[Ni(CN)_4]_3\}_\infty$ (**1**)[2f] and $\{(DMA)_4Yb[Ni(CN)_4]Cl\}_\infty$ (**2**).[2g] Despite rigorous attempts to remove oxygen and water from the system, oxidation of Yb^{2+} to Yb^{3+} occurs. The oxidation of Yb^{2+} by water can be discounted for two reasons. First, no OH stretching absorptions resulting from the formation of hydroxide-containing species are observed in the infrared spectra of any of the products. Second, the reduction of water would involve the evolution of hydrogen gas, which is not observed. The oxidation of divalent ytterbium may be explained from the formation of what is believed to be the Ni(I)-containing species $Ni_2(CN)_6^{4-}$. The IR spectra in Nujol mulls of the precipitates from the reaction in DMF and the reaction in DMA are consistent with the IR spectra reported[11] for $Ni_2(CN)_6^{4-}$, suggesting that $Ni(CN)_4^{2-}$ is acting as the oxidizing agent in this case. It is not surprising that formation of this dinuclear Ni(I) tetraanion occurs, since the estimated aqueous reduction potential of this system is 0.55 V (eqs 3−5).[12,13] Therefore, if the reduction potential of this

$$Yb^{3+} + 1e^- \rightarrow Yb^{2+} \qquad E^\circ = -1.10\ V^{12} \quad (3)$$

$$2Ni(CN)_4^{2-} + 2e^- \rightarrow Ni_2(CN)_6^{4-} + 2CN^- \qquad E^\circ = -0.55\ V^{13} \quad (4)$$

$$\text{net:}\quad 2Yb^{2+} + 2Ni(CN)_4^{2-} \rightarrow 2Yb^{3+} + Ni_2(CN)_6^{4-} + 2CN^- \qquad E^\circ = 0.55V \quad (5)$$

system does not change significantly by using solvents such as DMF and DMA, this redox reaction appears quite favorable. The insolubility of $Ni_2(CN)_6^{4-}$-containing species precluded any further characterization.

The europous ion is a weaker reducing agent than Yb(II). Compare the estimated aqueous reduction potentials of the two ions in eqs 3 and 6. The aqueous reduction potential of a reaction mixture containing $EuCl_2$ and $K_2Ni(CN)_4$ can be estimated to be −0.20 V (eqs 6−8). Neglecting solvent effects,

$$Eu^{3+} + 1e^- \rightarrow Eu^{2+} \qquad E^\circ = -0.35\ V^{12} \quad (6)$$

$$2Ni(CN)_4^{2-} + 2e^- \rightarrow Ni_2(CN)_6^{4-} + 2CN^- \qquad E^\circ = -0.55\ V^{13} \quad (7)$$

$$\text{net:}\quad 2Eu^{2+} + 2Ni(CN)_4^{2-} \rightarrow 2Eu^{3+} + Ni_2(CN)_6^{4-} + 2CN^- \qquad E^\circ = -0.20\ V \quad (8)$$

a similar reduction potential may be assumed in DMF. This negative potential indicates that oxidation of the europous ion is not favorable, contrary to what was observed with the reactions involving the use of Yb(II).

When equimolar amounts of $EuCl_2$ and $K_2M(CN)_4$ (M = Ni, Pt) are allowed to stir in DMF at room temperature for 2−3 days, the yellow-green solution turns bright yellow with the precipitation of KCl (eq 9). The formation of other precipitates

$$EuCl_2 + K_2M(CN)_4 \xrightarrow{DMF} (DMF)_xEuM(CN)_4 + 2KCl \quad (9)$$
$$M = Ni\ (\mathbf{3}),\ Pt\ (\mathbf{4})$$

is not observed, contrary to the findings in the analogous reactions between $YbCl_2$ and $K_2Ni(CN)_4$. Filtration followed by crystallization from these solutions results in the isolation of the Eu(II) solid state one-dimensional "ladders" having the formulas $\{(DMF)_4EuNi(CN)_4\}_\infty$ (**3**) and $\{(DMF)_4EuPt(CN)_4\}_\infty$ (**4**) as determined by single-crystal X-ray analyses.

Molecular Structures of $\{(DMF)_4EuNi(CN)_4\}_\infty$ and $\{(DMF)_4EuPt(CN)_4\}_\infty$. Crystallographic data for $\{(DMF)_4EuNi(CN)_4\}_\infty$ (**3**) and $\{(DMF)_4EuPt(CN)_4\}_\infty$ (**4**) are listed in Table 1. Tables 2 and 3 contain the positional parameters and equivalent isotropic thermal parameters for **3** and **4**, respectively. Table 4 lists selected bond distances and angles for **3** and **4**. Bright-yellow X-ray-quality crystals of $\{(DMF)_4EuNi(CN)_4\}_\infty$ were obtained from a concentrated DMF solution of **3** by slowly removing solvent under dynamic vacuum over several days. X-ray-quality crystals of $\{(DMF)_4EuPt(CN)_4\}_\infty$ were obtained in a slightly different manner. A concentrated DMF solution of **4** was warmed slightly using a warm water bath, and the solvent was removed under dynamic vacuum. Within 2 h,

Table 1. Crystallographic Data for $\{(DMF)_4EuNi(CN)_4\}_\infty$ and $\{(DMF)_4EuPt(CN)_4\}_\infty$

empirical formula	$C_{16}H_{28}N_8O_4EuNi$	$C_{16}H_{28}N_8O_4EuPt$
fw	607.10	743.50
space group	$P\bar{1}$	$P\bar{1}$
a, Å	8.902(2)	8.918(1)
b, Å	10.947(2)	11.160(2)
c, Å	12.464(4)	12.480(2)
α, deg	82.99(2)	83.27(2)
β, deg	86.86(2)	86.84(1)
γ, deg	84.92(2)	83.71(2)
V, Å^3	1199.6(5)	1225.0(4)
Z	2	2
ρ_{calcd}, g·cm^{-3}	1.681	2.016
T, °C	−60	−60
λ, Å	0.710 73 (Mo Kα)	0.710 73 (Mo Kα)
μ, cm^{-1} (calcd)	34.2	83.4
transm coeff	0.7590−0.9991	0.6319−0.9990
R_F[a]	0.022	0.022
R_{wF}[b]	0.026	0.025

[a] $R_F = \sum(|F_o| - |F_c|)/\sum|F_o|$. [b] $R_{wF} = [\sum w(|F_o| - |F_c|)^2/\sum w|F_o|^2]^{1/2}$, $w = [\sigma(F_o)^2 + (kF_o)^2]^{-1}$, $k = 0.04$.

(11) (a) El-Sayed, M. F. A.; Sheline, R. K. *J. Am. Chem. Soc.* **1956**, *78*, 702. (b) Griffith, W. P.; Wickham, A. *J. Chem. Soc. A* **1969**, 834.
(12) (a) Johnson, D. A. *J. Chem. Soc., Dalton Trans.* **1974**, 1671. (b) Morss, L. R. *Chem. Rev.* **1976**, *76*, 827.
(13) Hume, D. N.; Kolthoff, I. M. *J. Am. Chem. Soc.* **1950**, *72*, 4423.

Table 2. Positional Parameters and Their Esd's for $\{(DMF)_4EuNi(CN)_4\}_\infty$

atom	*x*	*y*	*z*	*B*,[a] Å^2
Eu	−0.11602(2)	1.25916(2)	−0.21836(1)	1.599(3)
Ni	−0.13273(5)	0.75648(4)	−0.17694(3)	1.725(8)
O1	0.1492(3)	1.1637(3)	−0.1952(2)	3.00(6)
O2	−0.3818(3)	1.3192(3)	−0.1499(3)	3.31(6)
O3	−0.2415(5)	1.3913(3)	−0.3772(3)	5.02(8)
O4	−0.0385(4)	1.1709(3)	−0.3958(2)	4.65(8)
N1	0.3416(4)	1.0209(3)	−0.1535(3)	2.32(6)
N2	−0.5813(4)	1.4551(3)	−0.1174(3)	2.38(6)
N3	−0.2760(5)	1.5121(3)	−0.5336(3)	3.68(8)
N4	−0.1660(4)	1.1178(3)	−0.5339(3)	3.19(7)
N11	−0.1883(4)	1.0300(3)	−0.1664(3)	2.65(7)
N12	−0.0732(4)	1.2477(3)	−0.0072(3)	2.58(6)
N13	−0.0484(4)	1.4882(3)	−0.2039(3)	3.11(7)
N14	−0.3769(5)	0.7632(4)	−0.3365(3)	4.29(9)
C1a	0.2036(4)	1.0712(4)	−0.1387(3)	2.46(7)
C1b	0.4402(5)	1.0709(4)	−0.2411(4)	3.7(1)
C1c	0.3988(5)	0.9094(4)	−0.0867(4)	3.48(9)
C2a	−0.4467(4)	1.4252(3)	−0.1589(3)	2.45(7)
C2b	−0.6469(6)	1.5821(4)	−0.1280(4)	3.61(9)
C2c	−0.6695(6)	1.3632(5)	−0.0571(4)	4.0(1)
C3a	−0.2265(6)	1.4891(4)	−0.4354(4)	4.0(1)
C3b	−0.3491(8)	1.4235(6)	−0.5831(4)	6.3(2)
C3c	−0.263(1)	1.6302(6)	−0.5987(5)	8.5(2)
C4a	−0.0550(6)	1.1672(5)	−0.4931(4)	4.0(1)
C4b	−0.1726(7)	1.1167(5)	−0.6493(4)	5.0(1)
C4c	−0.2845(8)	1.0687(6)	−0.4654(5)	6.5(2)
C11	−0.1726(4)	0.9251(3)	−0.1688(3)	2.03(7)
C12	−0.0011(4)	1.2480(3)	0.0662(3)	1.99(7)
C13	0.0798(4)	1.4100(3)	0.1920(3)	2.21(7)
C14	−0.2820(5)	0.7617(3)	−0.2781(3)	2.61(8)

[a] For Tables 2 and 3, anisotropically refined atoms are given in the form of the isotropic equivalent displacement parameter defined as (4/3)[$a^2B(1,1) + b^2B(2,2) + c^2B(3,3) + ab(\cos\gamma)B(1,2) + ac(\cos\beta)B(1,3) + bc(\cos\alpha)B(2,3)$].

Table 3. Positional Parameters and Their Esd's for $\{(DMF)_4EuPt(CN)_4\}_\infty$

atom	*x*	*y*	*z*	*B*,[a] Å^2
Pt	0.13333(3)	−0.25580(2)	0.17927(2)	1.581(4)
Eu	−0.11577(3)	−0.24221(2)	−0.22282(2)	1.631(5)
O1	−0.1479(5)	0.3394(4)	0.1926(4)	3.1(1)
O2	0.3845(6)	0.1787(4)	0.1617(4)	3.8(1)
O3	0.2289(8)	0.1065(5)	0.3823(4)	5.2(1)
O4	0.0367(7)	0.3334(5)	0.3979(4)	4.4(1)
N1	−0.3412(6)	−0.5188(4)	0.1515(4)	2.4(1)
N2	0.5794(6)	−0.9583(5)	0.1234(4)	2.5(1)
N3	0.2700(8)	−0.0165(5)	0.5366(4)	3.5(1)
N4	0.1739(7)	0.3818(5)	0.5319(4)	2.9(1)
N11	0.1901(6)	−0.5363(4)	0.1692(5)	2.7(1)
N12	−0.0827(7)	−0.2518(5)	−0.0111(4)	2.7(1)
N13	0.0493(7)	0.0210(4)	0.2025(5)	3.1(1)
N14	0.3815(8)	−0.2651(6)	0.3500(5)	4.4(1)
C1a	−0.2031(7)	−0.5693(6)	0.1367(5)	2.6(1)
C1b	−0.4000(9)	−0.4094(6)	0.0854(6)	3.4(2)
C1c	−0.4398(8)	−0.5671(6)	0.2385(6)	3.4(2)
C2a	0.4450(8)	−0.9262(6)	0.1657(5)	2.6(1)
C2b	0.6710(9)	−0.8699(8)	0.0670(7)	4.5(2)
C2c	0.6402(9)	−1.0852(7)	0.1287(6)	4.0(2)
C3a	0.217(1)	0.0103(6)	0.4405(6)	3.8(2)
C3b	0.262(2)	−0.1337(9)	0.5993(7)	6.8(3)
C3c	0.345(1)	0.0695(8)	0.5855(7)	5.9(2)
C4a	0.0576(8)	0.3398(7)	0.4937(5)	3.3(1)
C4b	0.294(1)	0.425(1)	0.4607(7)	6.0(2)
C4c	0.185(1)	0.3876(8)	0.6460(6)	4.3(2)
C11	0.1750(7)	−0.4338(5)	0.1711(5)	2.1(1)
C12	−0.0085(7)	−0.2506(5)	0.0621(5)	2.0(1)
C13	0.0798(7)	−0.0794(5)	0.1925(5)	2.2(1)
C14	0.2884(8)	−0.2628(5)	0.2897(5)	2.6(1)

yellow crystals of **4** began to form. When only a few milliliters of solvent remained, the system was isolated and allowed to stand at room temperature for 2 days.

Complexes **3** and **4** are isostructural and consist of one-dimensional "ladders" extending along the crystallographic *b* axis of the lattice. The asymmetric units of **3** and **4** consist of $[(DMF)_4EuM(CN)_4]$ fragments. By application of the symmetry operations of the space group to the $[(DMF)_4EuM(CN)_4]$ fragment and translation along the crystallographic *b* axis of the lattice, the one-dimensional "ladders" are generated. Figures 1 and 2 show a portion of each ladder for **3** and **4**, respectively. Figure 3 shows a unit cell packing diagram consisting of two parallel "ladders" for **3**. It is apparent that there are no close contacts between atoms of neighboring chains.

The coordination geometries of the Eu(II) ions in **3** and **4** consist of capped trigonal prisms (Figure 4). In each structure, the Eu(II) ions are coordinated to four DMF ligands through their oxygen atoms. In addition, each Eu(II) ion is coordinated by three different cyanide nitrogens from three different $M(CN)_4^{2-}$ ions, and each $M(CN)_4^{2-}$ ion in turn bridges three different Eu atoms through isocyanide linkages [Eu−NC−M]. The rungs of the ladder are created by one of the bridging cyano groups which caps one face of the trigonal prism. A similar Yb(II) "polymeric ladder" structure was reported by Deng and Shore[2b,c,e] where the rungs of the ladder are generated by direct Yb−Fe metal bonds.

The geometry of the $M(CN)_4^{2-}$ ions is approximately square planar, with C−M−C bond angles ranging from 88.1(1) to 91.4(2)° for **3** and from 87.7(2) to 91.6(2)° for **4**. The M−C bond distances range from 1.863(4) to 1.874(4) Å and from 1.977(6) to 1.998(6) Å in **3** and **4**, respectively. The C≡N bond distances range from 1.142(5) to 1.150(5) Å for **3** and from 1.140(8) to 1.159(8) Å for **4**. Although both the M−C and C≡N bonds vary with regard to both bridging and terminal modes, they are considered normal[10,14] with no statistically significant variations.

The M−C−N bond angles are almost linear and range from 174.3(3) to 178.3(3)° for **3** and from 174.9(6) to 178.5(6)° for **4**. However, the isocyanide linkages deviate significantly from linearity, causing a slight puckering of the ladder. They range from 152.9(3) to 154.2(3)° for **3** and from 151.1(5) to 153.8(6)° for **4**. This occurrence is also observed in a variety of analogous compounds containing $M-NCCH_3$ or M−OC linkages. It has been proposed that the angular position of the metal cation may allow for interaction with electron density of the lone pairs and π orbitals on CH_3CN or CO.[15] However, the energy gained or lost by the bending of the ligands might be sufficiently small that steric factors and crystal packing forces would facilitate the deviation from linearity in the $M-NCCH_3$ and M−OC linkages.

The Eu−N bond distances range from 2.641(3) to 2.666(3) Å and from 2.631(5) to 2.663(6) Å for **3** and **4**, respectively. Interestingly, the Eu−N12 bonds are significantly longer than both the Eu−N11 and Eu−N13 bonds. This observation is more pronounced in **4** than in **3**. These longer Eu−N bond distances are most likely attributed to the fact that the Eu−N12 bonds are generated by the bridging CN groups that form the rungs of the ladder and bringing the two edges of the ladder together might be sterically hindered by the DMF ligands. These distances are comparable to the average Eu−N bond distances (2.678 and 2.675 Å) of the coordinated acetonitrile ligands reported for the Eu(II) polymer $[closo\text{-}1,1,1\text{-}(MeCN)_3\text{-}1,2,4\text{-}EuC_2B_{10}H_{12}]_n$ containing two crystallographically independent molecules.[16] As expected, the Eu−N bond distances in **3** and **4** are longer than those involving eight-coordinate trivalent

(14) Cernak, J.; Dunaj-Jurco, M.; Melnik, M.; Chomic, J.; Skorsepa, J. *Rev. Inorg. Chem.* **1988**, *9*, 259.
(15) Darensbourg, M. Y. *Prog. Inorg. Chem.* **1985**, *33*, 221.

Table 4. Selected Bond Distances (Å) and Angles (deg) and Their Esd's for $\{(DMF)_4EuNi(CN)_4\}_\infty$ and $\{(DMF)_4EuPt(CN)_4\}_\infty$[a]

	distances			distances	
	$\{(DMF)_4EuNi(CN)_4\}_\infty$	$\{(DMF)_4EuPt(CN)_4\}_\infty$		$\{(DMF)_4EuNi(CN)_4\}_\infty$	$\{(DMF)_4EuPt(CN)_4\}_\infty$
M−C11	1.863(4)	1.994(6)	N1−C1b	1.448(5)	1.455(8)
M−C12	1.866(4)	1.977(6)	N1−C1c	1.459(5)	1.450(9)
M−C13	1.871(4)	1.998(6)	N2−C2a	1.309(5)	1.314(9)
M−C14	1.874(4)	1.995(7)	N2−C2b	1.454(5)	1.444(9)
Eu−O1	2.513(3)	2.508(5)	N2−C2c	1.443(6)	1.455(9)
Eu−O2	2.529(3)	2.526(5)	N3−C3a	1.311(6)	1.303(9)
Eu−O3	2.552(3)	2.540(5)	N3−C3b	1.431(7)	1.45(1)
Eu−O4	2.557(3)	2.550(5)	N3−C3c	1.451(7)	1.44(1)
Eu−N11	2.641(3)	2.631(5)	N4−C4a	1.320(6)	1.317(9)
Eu−N12	2.666(3)	2.663(6)	N4−C4b	1.444(6)	1.44(1)
Eu−N13	2.659(3)	2.644(5)	N4−C4c	1.421(7)	1.443(9)
O1−C1a	1.238(5)	1.237(8)	N11−C11	1.148(5)	1.140(8)
O2−C2a	1.244(5)	1.230(8)	N12−C12	1.146(5)	1.159(8)
O3−C3a	1.231(6)	1.235(9)	N13−C13	1.150(5)	1.144(8)
O4−C4a	1.236(5)	1.231(8)	N14−C14	1.142(5)	1.147(9)
N1−C1a	1.314(5)	1.310(8)			

	angles			angles	
	$\{(DMF)_4EuNi(CN)_4\}_\infty$	$\{(DMF)_4EuPt(CN)_4\}_\infty$		$\{(DMF)_4EuNi(CN)_4\}_\infty$	$\{(DMF)_4EuPt(CN)_4\}_\infty$
O1−Eu−O2	153.4(1)	153.4(2)	Eu−O1−C1a	133.0(3)	134.5(5)
O1−Eu−O3	131.9(1)	131.4(2)	Eu−O2−C2a	126.2(3)	125.8(5)
O1−Eu−O4	74.6(1)	75.9(2)	Eu−O3−C3a	139.5(4)	143.3(6)
O1−Eu−N11	83.7(1)	83.9(2)	Eu−O4−C4a	150.7(3)	149.5(5)
O1−Eu−N12	75.0(1)	74.8(2)	C1a−N1−C1b	120.8(3)	121.9(6)
O1−Eu−N13	95.0(1)	94.3(2)	C1a−N1−C1c	121.7(4)	120.9(6)
O2−Eu−O3	74.4(1)	74.7(2)	C1b−N1−C1c	117.4(3)	117.2(6)
O2−Eu−O4	126.8(1)	125.2(2)	C2a−N2−C2b	121.6(4)	121.6(6)
O2−Eu−N11	84.9(1)	84.3(2)	C2a−N2−C2c	121.2(4)	121.2(6)
O2−Eu−N12	79.9(1)	80.1(2)	C2b−N2−C2c	117.2(4)	117.3(6)
O2−Eu−N13	88.6(1)	88.7(2)	C3a−N3−C3b	122.4(4)	123.3(7)
O3−Eu−O4	69.4(1)	70.0(2)	C3a−N3−C3c	122.2(5)	120.9(6)
O3−Eu−N11	119.1(1)	121.7(2)	C3b−N3−C3c	115.4(5)	115.7(7)
O3−Eu−N12	143.4(1)	142.2(2)	C4a−N4−C4b	120.7(4)	121.0(6)
O3−Eu−N13	74.8(1)	74.0(2)	C4a−N4−C4c	120.7(4)	121.5(6)
O4−Eu−N11	80.2(1)	80.3(2)	C4b−N4−C4c	118.6(5)	117.5(7)
O4−Eu−N12	146.7(1)	147.4(2)	Eu−N11−C11	154.2(3)	153.8(5)
O4−Eu−N13	116.8(1)	118.8(2)	Eu−N12−C12	153.9(3)	151.1(5)
N11−Eu−N12	83.5(1)	82.6(2)	Eu−N13−C13	152.9(3)	153.5(6)
N11−Eu−N13	162.1(1)	159.9(2)	O1−C1a−N1	123.9(4)	123.9(7)
N12−Eu−N13	78.9(1)	77.7(2)	O2−C2a−N2	125.0(4)	124.8(6)
C11−M−C12	88.1(1)	87.7(2)	O3−C3a−N3	123.3(5)	125.2(8)
C11−M−C13	175.6(2)	176.5(3)	O4−C4a−N4	125.5(5)	126.1(7)
C11−M−C14	90.6(2)	91.1(2)	M−C11−N11	175.8(4)	175.8(6)
C12−M−C13	91.4(2)	91.6(2)	M−C12−N12	174.3(3)	174.9(6)
C12−M−C14	174.6(2)	175.9(3)	M−C13−N13	178.3(3)	178.5(6)
C13−M−C14	90.3(2)	89.9(2)	M−C14−N14	177.3(4)	177.3(7)

[a] Bond distances and angles were calculated for symmetry-related atoms by applying the inversion operation.

Eu ions containing isocyanide linkages in the complexes $(H_2O)_{12}Eu_2[Pd(CN)_4]_3$ (2.530 Å)[9] and $\{(DMF)_xEu_2[Ni(CN)_4]_3\}_\infty$ (2.523 Å).[2g]

The Eu−O bond distances of the coordinated DMF ligands range from 2.513(3) Å to 2.557(3) and from 2.508(5) Å to 2.550(5) Å for **3** and **4**, respectively. Interestingly, the Eu−O3 and Eu−O4 bond distances are significantly longer than the Eu−O1 and Eu−O2 bond distances in both **3** and **4**. This can be attributed to the fact that both DMF ligands corresponding to O3 and O4 share edges with two DMF ligands, increasing the steric hindrance of that coordination site. On the other hand, the DMF ligands corresponding to O1 and O2 share an edge with only one other DMF ligand. As expected, these distances are longer than the average bond distances found in the eight-coordinate Eu(III) one-dimensional array $\{(DMF)_xEu_2[Ni(CN)_4]_3\}_\infty$ (2.361 Å)[2g] and the seven-coordinate Yb(II) carborane complex $(DMF)_4Yb(C_2B_9H_{11})$ (2.37 Å).[17] Seven-coordinate Yb(II) is reported to be 0.12 Å smaller than seven-coordinate Eu(II).[18]

Spectroscopic and Solution Studies. The Nujol infrared spectra of **3** and **4** display similar absorption patterns, with the peaks of **4** shifted to higher energies as expected (Figure 5).[19] The spectrum of **3** shows four cyanide stretching vibrations at 2146 (w), 2140 (m), 2127 (s), and 2117 (s) cm^{-1}, and those of **4** appear at 2170 (w), 2154 (m), 2139 (s), and 2130 (s) cm^{-1}. Group theory predicts that only one absorption in the infrared spectrum due to CN stretching should occur for square planar tetracyanometalates(II) having D_{4h} symmetry. Isocyanide linkages to the Eu(II) ions in **3** and **4** lower the symmetry of the square planar $Ni(CN)_4^{2-}$ and $Pt(CN)_4^{2-}$ ions, resulting in the observed multiple CN stretching absorptions.

(16) Khattar, R.; Manning, M. J.; Knobler, C. B.; Johnson, S. E.; Hawthorne, M. F. *Inorg. Chem.* **1992**, *31*, 268.

(17) Manning, M. J.; Knobler, C. B.; Khattar, R.; Hawthorne, M. F. *Inorg. Chem.* **1991**, *30*, 2009.

(18) Shannon, R. D. *Acta Crystallogr.* **1976**, *A32*, 751.

(19) Nakamoto, K. *Infrared and Raman Spectra of Inorganic and Coordination Compounds*, 4th ed.; Wiley: New York, 1986; see also references therein.

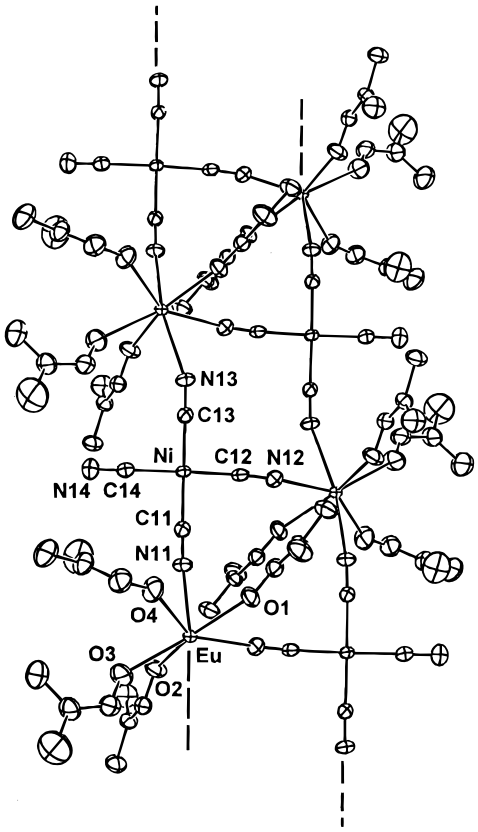

Figure 1. ORTEP drawing (50% thermal ellipsoids) of a portion of the one-dimensional "ladder" in $\{(DMF)_4EuNi(CN)_4\}_\infty$.

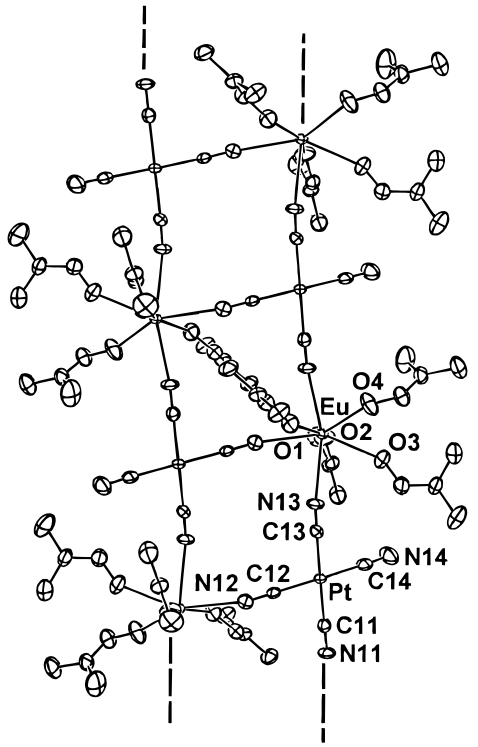

Figure 2. ORTEP drawing (50% thermal ellipsoids) of a portion of the one-dimensional "ladder" in $\{(DMF)_4EuPt(CN)_4\}_\infty$.

When **4** was placed under dynamic vacuum for 12−14 h, elemental analysis showed that two coordinated DMF ligands were removed per molecule to give $[(DMF)_2EuPt(CN)_4]_\infty$ (**4a**). This corresponds to a change in the solid state infrared spectrum, and only two ν_{CN} absorptions are observed at 2148 (s, br) and 2110 (w, sh) cm^{-1} (Figure 6). Under conditions

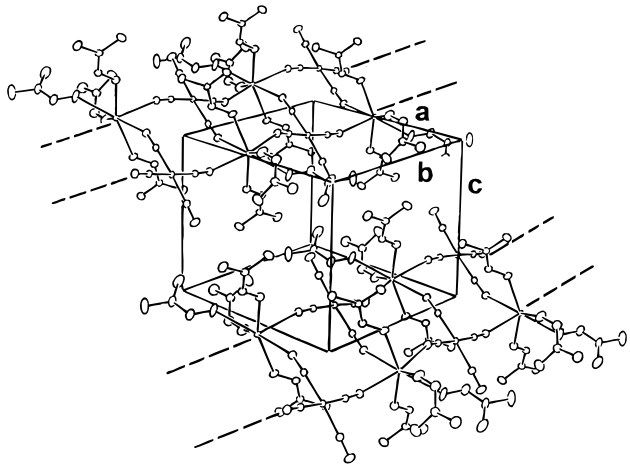

Figure 3. Unit cell packing diagram for $\{(DMF)_4EuNi(CN)_4\}_\infty$.

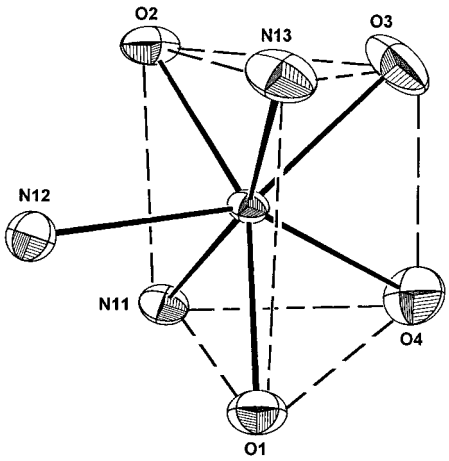

Figure 4. Capped trigonal prism geometry of Eu(II) in $\{(DMF)_4EuNi(CN)_4\}_\infty$.

identical to those above, **3** yields $[(DMF)_2EuNi(CN)_4]_\infty$ (**3a**) having an infrared spectrum similar to that of **4a** (Figure 6). Again, the observed CN stretching absorptions of **3a** at 2138 (s) and 2097 (vw) cm^{-1} are at lower energies than those observed for **4a**. The simpler infrared spectra observed for **4a** and **3a** suggest that removal of the coordinated DMF ligands enable the $M(CN)_4^{2-}$ anions to approach ideal square planar geometry.

Infrared spectra of **3** and **4** in DMF suggest that the one-dimensional ladders are not preserved in solution and possible ionization occurs (Figure 7). Complex **3** shows two CN stretching absorptions at 2114 (s) and 2137 (w) cm^{-1}, while **4** shows two absorptions at 2122 (s) and 2160 (vw) cm^{-1}. The absorptions at 2137 and 2160 cm^{-1} suggest that some ion-pairing is occurring in solution (eq 10). Compare these spectra

$$(DMF)_xEu(NC)M(CN)_3 + n\text{DMF} \rightleftharpoons (DMF)_{x+n}Eu^{2+} + M(CN)_4^{2-} \quad (10)$$

with the DMF solution spectra of $K_2Ni(CN)_4$ (2113 cm^{-1}) and $K_2Pt(CN)_4$ (2122 cm^{-1}) where complete ionization takes place. The intensity of the absorption at 2160 cm^{-1} observed for **4** is weaker than the comparable absorption at 2137 cm^{-1} of the nickel analog. This implies that the ion-pairing is greater in solutions of **3** than in those of **4**. This is confirmed by solution electrical conductance measurements in DMF. At 1 mM concentrations, the molar conductivities of **3** and **4** are 55 and 60 $cm^2\ \Omega^{-1}\ mol^{-1}$, respectively. These conductivities are slightly lower than those expected for a completely ionized 1:1

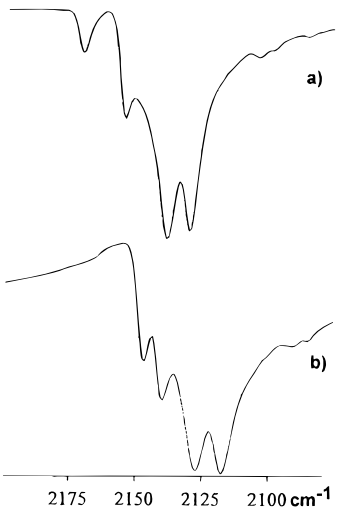

Figure 5. Nujol infrared spectra of (a) $\{(DMF)_4EuPt(CN)_4\}_\infty$ and (b) $\{(DMF)_4EuNi(CN)_4\}_\infty$ in the ν_{CN} absorption region.

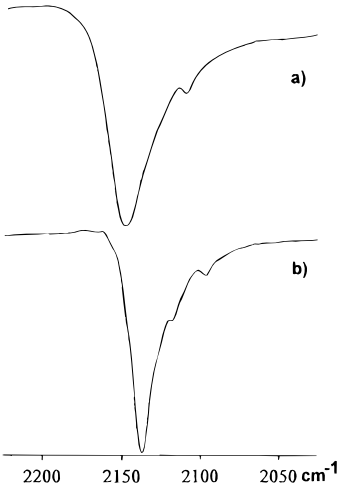

Figure 6. Nujol infrared spectra of (a) $\{(DMF)_2EuPt(CN)_4\}_\infty$ and (b) $\{(DMF)_2EuNi(CN)_4\}_\infty$ in the ν_{CN} absorption region.

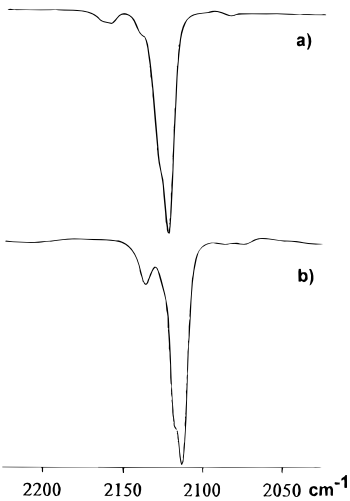

Figure 7. DMF solution infrared spectra of (a) $\{(DMF)_4EuPt(CN)_4\}_\infty$ and (b) $\{(DMF)_4EuNi(CN)_4\}_\infty$ in the ν_{CN} absorption region.

electrolyte in DMF[20] and confirm that some ion-pairing occurs in solutions of **3** and **4**. The lower conductivity of **3** compared to **4** also verifies that ion-pairing is more prominent in solutions of **3**, resulting in a shift to the left in the equilibrium (eq 10). This is expected because the smaller size of the $Ni(CN)_4^{2-}$ anion allows for stronger interactions with the Eu(II) cation. It also appears, from comparison to studies involving trivalent lanthanides in DMF solutions with tetracyanometalate(II) anions,[2g] that in DMF solution the tetracyanometalate(II) anions prefer coordination to the harder Lewis acids. The paramagnetism of Eu(II) prohibited any investigations employing NMR techniques.

Experimental Section

General Data. All manipulations were carried out on a standard high-vacuum line or in a drybox under an atmosphere of dry, pure N_2. NH_3 (Matheson) was dried over sodium and distilled prior to use. DMF (Baker) was stirred over pretreated 4 Å molecular sieves for 4−5 days in a Pyrex flask. The DMF was then degassed under vacuum, and the flask was connected to a U-tube apparatus in the drybox. The DMF was degassed a second time under vacuum and then distilled at 70−80 °C into a 1000 mL Pyrex flask at −78 °C. The DMF was then stored in the drybox. DMA (Aldrich) was stirred over BaO for 4−5 days in a Pyrex flask. The DMA was then degassed under vacuum, and the flask was connected to a U-tube apparatus in the drybox. The DMA was degassed a second time under vacuum and then distilled at 70−80 °C into a 1000 mL Pyrex flask at −78 °C. The DMA was then stored in the drybox. Linde brand molecular sieves (4 Å) were heated to 150 °C under dynamic vacuum for 12−24 h prior to use.

Carbon-13 NMR spectra were obtained on a Bruker AM-250 NMR spectrometer operating at 62.90 MHz. Chemical shifts for ^{13}C NMR spectra were internally referenced to carbon-13 peaks (δ(TMS) = 0.00 ppm). Fourier transform infrared (FTIR) spectra were recorded on a Mattson Polaris Fourier transform spectrometer with 2 cm^{-1} resolution. Samples were prepared as solutions or Nujol mulls. Nujol samples were analyzed as films placed between KBr plates in an airtight sample holder. Solution spectra were obtained using airtight Perkin-Elmer cells with 0.1 mm Teflon spacers between KBr or NaCl windows. All IR samples were prepared in the drybox.

Elemental analyses of materials were performed by Oneida Research Services, Inc., Whitesboro, NY. Conductance measurements were obtained using a YSI Model 35 conductance−resistance meter equipped with a YSI Model 3401 dip cell. All measurements were performed in the drybox employing standardized solutions in DMF.

Yb and Eu, 40 mesh (Strem), were used as received. $K_2Ni(CN)_4 \cdot H_2O$ (Strem) was dried under vacuum at 150 °C for 16 h and stored in the drybox. $K_2Pt(CN)_4$ (Strem) was dried under vacuum for 8−10 h and stored in the drybox. $(NH_3)_xEuCl_2$ and $(NH_3)_xYbCl_2$ were prepared from Eu and Yb metal, respectively, and NH_4Cl in liquid ammonia by the method of Howell and Pytlewski.[21] Hydrogen gas was collected *via* a calibrated Toepler pump in order to determine the yields of $(NH_3)_xEuCl_2$ and $(NH_3)_xYbCl_2$.

Reactions of $YbCl_2$ with $K_2Ni(CN)_4$. (a) In DMF. In the drybox, approximately 10 mL of dry DMF was added to 0.542 mmol of $(NH_3)_xYbCl_2$ to form an orange solution. To this solution was added 130 mg (0.542 mmol) of $K_2Ni(CN)_4$. The mixture was stirred under N_2, and the color of the solution changed to a dark brown within 20−30 min. After being stirred several days, the reaction mixture was filtered, leaving a brown precipitate. An X-ray powder pattern showed that the precipitate contained KCl. IR of precipitates (Nujol mull, ν_{CN}, cm^{-1}): 2146 (m), 2122 (m−s), 2066 (vs). The filtrate was light yellow and was identified as $\{(DMF)_{10}Yb_2[Ni(CN)_4]_3\}_\infty$. IR (Nujol mull of crystals, ν_{CN}, cm^{-1}): 2164 (s, sh), 2160 (s), 2150 (s), 2122 (vs), 2110 (m, unresolved). IR (DMF solution, ν_{CN}, cm^{-1}): 2150 (m−s), 2123 (vs), 2115 (vs), 2113 (s, unresolved). $^{13}C\{^1H\}$ NMR (DMF, 303K, δ (ppm)): 129.68 (s). This compound loses one DMF per formula unit in vacuum at room temperature. Anal. Calcd for $C_{39}H_{63}N_{21}Ni_3O_9Yb_2$: C, 31.39; H, 4.25; N, 19.71. Found: C, 31.11; H, 3.94; N, 19.41.

(b) In DMA. In the drybox, approximately 25 mL of dry DMA was added to 0.578 mmol of $(NH_3)_xYbCl_2$, dissolving the ytterbium dichloride and giving an orange solution. To this solution was added 139 mg (0.578 mmol) of $K_2Ni(CN)_4$. The mixture was stirred under N_2, and the color of the solution changed to brown within 20−30 min.

(20) Geary, W. *J. Coord. Chem. Rev.* **1971**, *7*, 81.

(21) Howell, J. K.; Pytlewski, L. L. *J. Less-Common Met.* **1969**, *18*, 437.

After 48 h, the solution turned orange. The reaction mixture was filtered, leaving a light orange precipitate. An X-ray powder pattern showed that the precipitate contained KCl. IR of precipitates (Nujol mull, ν_{CN}, cm^{-1}): 2141 (w), 2117 (w), 2099 (vw), 2055 (vs, br). The filtrate was light yellow and was identified as $\{(DMA)_4Yb[Ni(CN)_4]Cl\}_\infty$. IR (Nujol mull of crystals, ν_{CN}, cm^{-1}): 2208 (vw), 2159 (w), 2140 (s), 2117 (s). IR (DMA solution, ν_{CN}, cm^{-1}): 2146 (vw), 2112 (s).

Preparation of $[(DMF)_4EuNi(CN)_4]_\infty$. In the drybox, 0.428 mmol of $(NH_3)_xEuCl_2$ was dissolved in dry DMF to form a green solution. To this solution was added 103 mg (0.428 mmol) of $K_2Ni(CN)_4$, and the mixture was stirred. After 3 days, the solution was filtered, leaving a white precipitate on the frit (KCl) and a yellow filtrate solution. The solvent was removed, leaving a yellow powder. IR of powder (Nujol mull, ν_{CN}, cm^{-1}): 2138 (s), 2097 (vw). IR (DMF solution, ν_{CN}, cm^{-1}): 2114 (s), 2137 (w).

X-ray-quality crystals of $[(DMF)_4EuNi(CN)_4]_\infty$ were obtained by dissolving a freshly prepared sample of $[(DMF)_xEuNi(CN)_4]_\infty$ in DMF. Solvent was removed slowly under vacuum over several days until yellow crystals were obtained. IR (Nujol mull, ν_{CN}, cm^{-1}): 2146 (w), 2140 (m), 2127 (s), 2117 (s).

Preparation of $[(DMF)_4EuPt(CN)_4]_\infty$. In the drybox, 0.400 mmol of $(NH_3)_xEuCl_2$ was dissolved in dry DMF to form a green solution. To this solution was added 149 mg (0.389 mmol) of $K_2Pt(CN)_4$, and the mixture was stirred. After 3 days, the solution was filtered, leaving a white precipitate on the frit (KCl) and a yellow filtrate solution. X-ray-quality crystals of $[(DMF)_4EuPt(CN)_4]_\infty$ were obtained as follows. A concentrated DMF solution was warmed slightly using a warm water bath, and the solvent was removed under dynamic vacuum. Within 2 h, yellow crystals began to form. When only a few milliliters of solvent remained, the system was isolated and allowed to stand at room temperature for 2 days. Yield: nearly quantitative. IR (Nujol mull, ν_{CN}, cm^{-1}): 2170 (w), 2154 (m), 2139 (s), 2130 (s). The crystals were dried under dynamic vacuum for 12−14 h, yielding $[(DMF)_2EuPt(CN)_4]_\infty$. Anal. Calcd for $C_{10}H_{14}EuN_6O_2Pt$: C, 20.11; H, 2.36; N, 14.07. Found: C, 19.80; H, 2.17; N, 13.72. IR (Nujol mull ν_{CN}, cm^{-1}): 2148 (s, br), 2110 (w, sh). IR (DMF solution, ν_{CN}, cm^{-1}): 2122 (s), 2160 (vw).

X-ray Structure Determination of $[(DMF)_4EuNi(CN)_4]_\infty$ and $[(DMF)_4EuPt(CN)_4]_\infty$. Suitable single crystals were mounted and sealed inside glass capillaries of 0.3 or 0.5 mm diameter. Single-crystal X-ray diffraction data were collected on an Enraf-Nonius CAD4 diffractometer using graphite-monochromated molybdenum Kα radiation. The diffractometer was equipped with a dry air refrigeration unit for collection of data at low temperature. Unit cell parameters were obtained by a least-squares refinement of the angular settings from 25 reflections, well distributed in reciprocal space and lying in the 2θ range of 24−30°. Crystallographic data are given in Table 1, positional and equivalent isotropic thermal parameters are given in Tables 2 and 3, and bond distances and angles are given in Table 4.

The diffraction data were corrected for Lorentz and polarization effects, decay, and absorption (empirically from ψ-scan data). Computations were performed on a VAXstation 3100 computer using MOLEN.[22] Structures were solved using the direct method MULTAN 11/82 and difference Fourier synthesis with analytical scattering factors used throughout the structure refinement.[23] Both real and imaginary components of the anomalous dispersion were included for all non-hydrogen atoms. After all of the non-hydrogen atoms were located and refined, hydrogen atoms on the DMF ligands were placed at calculated positions by assuming ideal geometries with C−H distances of 0.95 Å. The thermal parameters of the hydrogen atoms were set to $B(H) = 1.3B(C)$ Å^2. Then, with the positional and thermal parameters of all of the hydrogen atoms fixed, the non-hydrogen atoms were refined anisotropically. New hydrogen positions were calculated, and this procedure was repeated until the parameters of the non-hydrogen atoms were refined to convergence (final shift/error ≤ 0.03). The highest residual peaks on the final difference Fourier maps were 0.981 e/Å^3 at a distance of 0.950 Å from Eu in **3** and 1.499 e/Å^3 at a distance of 1.004 Å from Pt in **4**.

Acknowledgment. This work was supported by the National Science Foundation through Grant CHE 94-0123.

Supporting Information Available: Listings of crystallographic data, positional parameters, anisotropic thermal parameters, bond distances, and bond angles (13 pages). Ordering information is given on any current masthead page.

IC960337V

(22) MOLEN, an interactive structure solution procedure developed by Enraf-Nonius, Delft, The Netherlands (1990), was used to process X-ray data, to apply corrections, and to solve and refine structures.

(23) Atomic scattering factors from: *International Tables for X-ray Crystallography*; Kynoch: Birmingham, U.K., 1974; Vol IV.